Formation and Reductive Desorption of Mercaptohexanol Monolayers on Mercury

Juan José Calvente,* Rafael Andreu,* Lucía González, María-Luisa A. Gil, Juan Daniel Mozo, and Emilio Roldán

Departamento de Química Física. Facultad de Química, Universidad de Sevilla, 41012 Sevilla, Spain

Received: December 31, 2000; In Final Form: March 23, 2001

The formation and reductive desorption of self-assembled monolayers of 6-mercaptohexanol on mercury has been studied by using cathodic stripping voltammetry and capacitative transients, including the possibility of expanding or contracting the electrode area at the end of the preconcentration step. Experimental evidence shows the existence of three sequential stages during the formation of a thiol self-assembled monolayer. Each of these stages can be associated to the presence of (i) a low surface density state of oxidized thiol molecules, characterized by a single electrodimerization wave, (ii) a high surface density state, characterized by the emergence of a second voltammetric wave, and (iii) an ordered monolayer, which gives rise to a voltammetric spike. On the basis of electrode expansion experiments, a method is described to determine the surface concentrations of oxidized products, which does not require a baseline subtraction of the voltammograms to account for the nonfaradaic current. Quantitative voltammetric fits are consistent with the initial formation of a mixture of noninteracting monomers and dimers of oxidized thiol. The value of the maximum surface concentration and the ability to block the $Ru(NH_3)_6^{3+}$ electron transfer reveal that oxidized thiol molecules adopt a nearly perpendicular orientation in the high surface density state, which hampers ionic permeation. A theoretical model is proposed to account for the observed voltammetric behavior. The transition from the lower to the higher surface density states is modeled as a chemical step involving the exchange of metal free sites. Capacitative transients are also interpreted in terms of the three-stages model.

Introduction

Organothiols display a high affinity toward metallic surfaces (such as Au, Ag, Hg, etc.), and simultaneously, they possess the ability to reorient themselves in the adsorbed state. These two characteristics have been exploited to build long-range structured films, known as self-assembled monolayers (SAMs).[1−3] Besides their technological importance, these systems serve as prototypes for studying fundamental issues such as electron tunneling or ionization of surface-anchored acid/base and redox groups.

Although most studies on SAMs have been performed on gold substrates, particularly Au(111) single crystals, mercury also offers some advantages derived from the reproducibility and the atomically flat character of its liquid surface, which seems to facilitate the formation of SAMs with a very low density of defects.[4−6] This feature has allowed the differentiation between racemic and pure enantiomeric SAMs.[7] Mercury also offers the possibility of expanding or contracting the substrate surface at any stage during the thiol deposition process. This strategy has been applied by Bruckner-Lea et al.[8] to mimic Langmuir−Blodgett experiments with an octanethiol film adsorbed on a variable surface area sessile mercury drop and to introduce or remove defects in the insulating film.[9] Recently, Majda and co-workers[10−12] have used gradual expansion experiments with alkanethiol-coated hanging mercury electrodes to investigate the influence of the monolayer thickness on the rate of electron tunneling across the interface.

Within the electroanalytical field, the high affinity of thiols toward mercury has allowed the development of electrochemical stripping protocols to determine low concentrations of dissolved thiols[13] and to exploit the ion-exchange properties of mercaptocarboxylic acids adsorbed on mercury to detect the presence of Cd^{2+} traces in solution.[14]

Despite the extensive literature, there is not yet a clear picture for the mechanism of the thiol self-assembling process on mercury. Early electrochemical studies in this field started with the seminal work of Kolthoff and co-workers[15] on the polarographic behavior of cysteine and glutathione. The two observed anodic waves were interpreted in terms of the formation of a submonolayer and a monolayer, respectively, of the corresponding mercurous thiolate (Hg(SR)). However, this assignment has been controversial because a later report of Miller and Teva[16] ascribed the double wave to the presence of both mercurous (Hg(SR)) and mercuric thiolate ($Hg(SR)_2$) in the adsorbed layer, whereas Stankovich and Bard[17] proposed an interpretation in terms of the formation of adsorbed $Hg(SR)_2$ and its transition to a compact film. In a later study on the electrochemical detection of low molecular weight thiols, Birke and Mazorra[18] reported on the formation of a $Hg(SR)_2$ multilayer film at anodic potentials, when high concentrations of thiol were used. Moreover, evidence for the presence of mercuric thiolates in solution was also given in some of these studies.

In recent years, the mechanistic aspects of the oxidative adsorption of thiols on mercury have been reassessed, because

* To whom correspondence should be addressed. Phone: +34-954557177. Fax: +34-954557174. E-mail: fondacab@cica.es. E-mail: pacheco@cica.es.

10.1021/jp0045991 CCC: $20.00
Published on Web 05/17/2001

of the fundamental and technological applications of SAMs. Mandler and co-workers[6,19] have studied the formation of SAMs of *n*-alkanethiols and *ω*-mercaptocarboxylic acids on mercury. They reported on the existence of thiol molecules in a physisorbed state at potentials more negative than the redox wave and on the formation of chemisorbed multilayers at more positive potentials. They also described the occurrence of a surface reorganization process, which leads to a densely packed structure of oxidized thiol molecules. White and co-workers[20] obtained three voltammetric waves during the oxidative adsorption of short *n*-alkanethiols ($n \leq 5$) and only two waves in the oxidation of the longer alkanethiols ($n > 5$). They also demonstrated that a critical value of the hydrocacarbon chain length sets the limit for the formation of either multilayers ($n \leq 5$) or densely packed monolayers ($n > 5$). They ascribed the two more anodic waves to the formation of energetically distinct low- and high-density surface phases and the third wave to the deposition of a bulk film of mercurous or mercuric thiolate. It is interesting to note the close similarity between the oxidative adsorption of thiols on mercury and silver, where the low- and high-density phases were probed by Raman spectroscopy (SERS) and electrochemical quartz crystal microbalance (EQCM) measurements.[21,22]

In a previous report, we have described the electrochemical oxidation of a submonolayer of 2-mercaptoethyl ether.[23] Under conditions where the surface process could be isolated from the solution, the formation of a dimeric species (either $Hg_2(SR)_2$ or $Hg(SR)_2$) was demonstrated quantitatively. Later, a study on the reductive desorption of submonolayers of oxidized *ω*-mercaptocarboxylic acids on mercury was performed by using cathodic stripping voltammetry.[24] It was found that in alkaline media the Hg(SR) monomer is formed, whereas in acid solutions, the oxidation products are the $Hg_2(SR)_2$ or $Hg(SR)_2$ dimers.

In this paper, we explore some mechanistic aspects of thiol oxidation, related to the increase of its surface concentration and, eventually, to the electrochemical building of a SAM. We have selected mercaptohexanol for our study as a compromise between the short alkanethiols, that form either multilayers or partially soluble monolayers upon oxidation, and the longer alkanethiols, which are hardly soluble in water. It is shown how a precise control over the rate of formation of a thiol monolayer can be achieved by combining a potential step perturbation, to trigger the deposition process at positive potentials, and the use of low concentrations of thiol in solution, to increase the required preconcentration time up to $\sim 10^2$ s. Such an extended time scale offers the possibility of extracting detailed information, in the form of cathodic stripping voltammograms, on the successive physical stages that lead to the formation of a thiol SAM. Quantitative analysis of the stripping voltammograms provides information on the nature (monomers vs dimers), amount, and orientation of the adsorbed molecules. Additional structural information is obtained from differential capacity measurements, the effect of a gradual contraction/expansion of the electrode area, and the study of the blocking properties of adsorbed structures on the heterogeneous electron transfer of $Ru(NH_3)_6^{3+}$. As a result, a step-by-step picture of the surface aggregation process that leads to the monolayer self-assembly is presented.

Experimental Section

Background solutions of 0.5 M NaOH and 0.5 M H_3PO_4 + 0.06 M $NaClO_4$ at pH 7 were prepared from Merck (p.a.) reagents and water purified with a Millipore Milli-Q system. 6-Mercapto-1-hexanol (MHOL) and $Ru(NH_3)_6Cl_3$ were purchased from Fluka and Alfa-Aesar, respectively, and used without further purification. Mercury was distilled three times under vacuum after treatment with diluted nitric acid and mercurous nitrate.

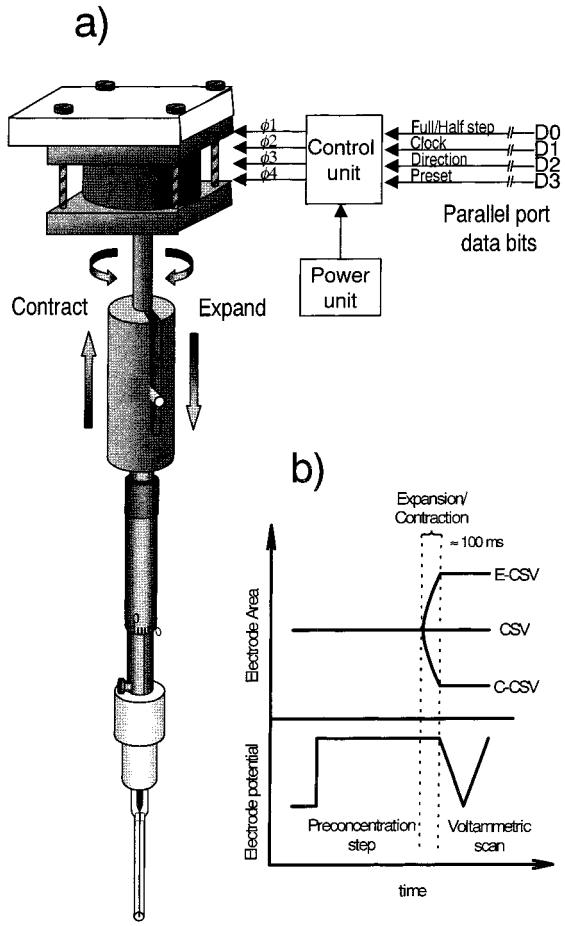

Figure 1. (a) Scheme of the motor-driven hanging mercury electrode (HMDE), allowing for an expansion/contraction of the electrode surface at the end of the preconcentration time. (b) Electrode surface area and potential profiles for classical (CSV), expanding (E-CSV), and contracting (C−CSV) cathodic stripping voltammetries.

Electrochemical measurements were carried out in a three electrode, water-jacketed glass cell, thermostated at 25 ± 0.2 °C with a Haake D8.G circulator thermostat. Solutions were deaerated with a nitrogen stream prior to the measurements.

A sodium saturated calomel electrode and a platinum foil were used as reference and auxiliary electrodes, respectively. The working electrode was a stepper-motor driven hanging mercury drop electrode, which allows for expansion or contraction of its surface area at a preset time (Figure 1a). It was built by assembling a Kemula-Kublik type HMDE (Mineral, Poland) to a stepper motor (RS 440-436) via a home-built slotted keyway drive coupling made of nylon. The motor was connected to the Centronics port of a 386 personal computer via a 4-phase unipolar drive board (RS217-3611). Four logic lines were used for its digital control. D0 sets the maximum values of both the resolution (0.6°/step) and rotation speed (500 step/s). D1 sets the clock frequency (actual rotation speed) and the number of pulses (extension of the electrode surface area change). D2 sets the direction of the rotation (expansion or contraction), and D3 sets the initial polarization of the four coils. The synchronization between the stepper motor and the potentiostat was controlled by a QBASIC program, to produce potential and electrode area profiles such as those depicted in Figure 1b. The drop area corresponding to a given number of divisions of the micrometric

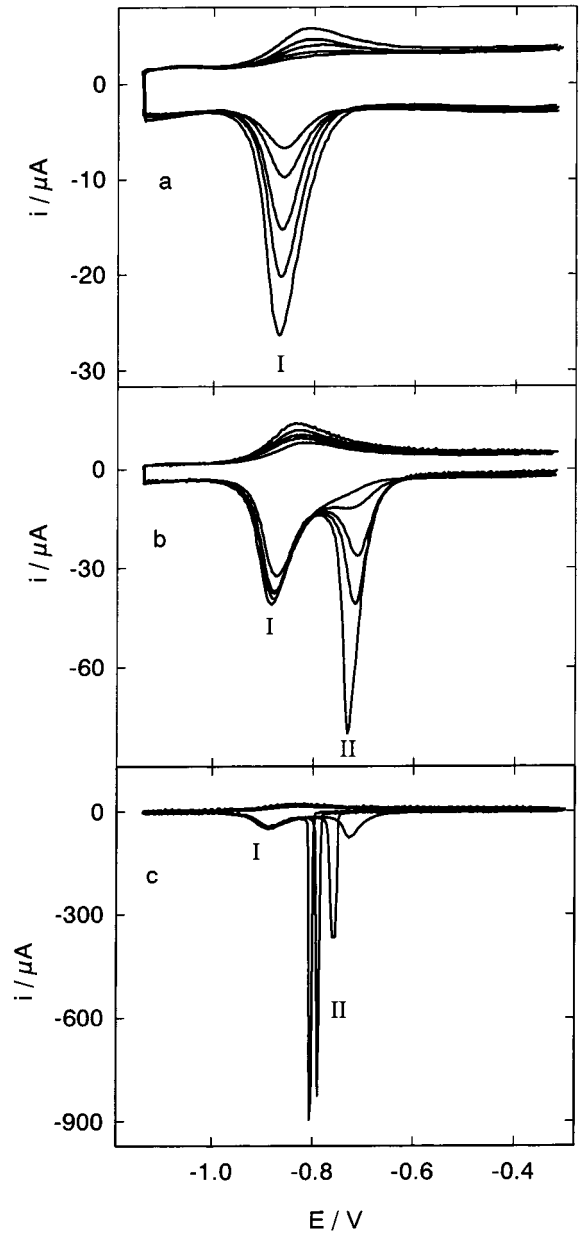

Figure 2. Cathodic stripping voltammograms corresponding to a 20 μM MHOL solution in 0.5 M NaOH, as a function of the preconcentration time. From top to bottom (a) τ = 1, 2, 5, 10, and 15 s; (b) τ = 30, 40, 50, 70, and 90 s; and (c) τ =100, 130, 150, and 200 s. Scan rate v = 10 V s^{-1}and preconcentration potential E_i = −0.3 V (SSCE).

head was calibrated by weighing three sets of 10 drops. The electrode area was varied within the 8×10^{-3} cm$^2 \leq A \leq 0.039$ cm^2 range.

Voltammetric measurements were performed with a CAEM PGA1210 potentiostat/generator coupled to a digital acquisition system. Impedance measurements were carried out with an Autolab PGSTAT30 manufactured by Eco Chemie. Differential capacity values were found to be independent of the perturbation frequency in the 320 Hz−4020 Hz range.

Results and Discussion

Stripping voltammograms of oxidized MHOL are characterized by the presence of either one or two cathodic waves. Figure 2 illustrates the evolution of the voltammetric response as the preconcentration time τ increases, for a 20 μM MHOL solution in 0.5 M NaOH. The preconcentration potential was held at −0.3 V in these experiments, to produce a diffusion-limited deposit of oxidized thiol on mercury. Once the preset time τ had elapsed, the potential was swept cathodically at a 10 V s^{-1} scan rate, to obtain the reductive desorption voltammogram. Three types of voltammetric behavior can be identified upon increasing the preconcentration time. At low preconcentration times (Figure 2a) a single voltammetric wave (wave I) is obtained; its width varies within the 73 mV−85 mV range, and its peak potential shifts toward more negative values as the MHOL surface concentration increases. As soon as the charge under wave I reaches a critical value of 30 ± 2 μC cm^{-2}, whatever the preconcentration time and thiol concentration, an additional voltammetric wave (wave II) develops at more positive potentials (Figure 2b), corresponding to an electrochemically less stable state of the oxidized MHOL molecule. The narrowness of wave II, as compared with wave I, is indicative of an attractive interaction between the adsorbed molecules.[25] It should also be pointed out that wave I does not change as far as wave II is present, and it remains insensitive to the specific features of wave II. Eventually, at long enough preconcentration times, the overall charge under waves I and II reaches a limit of 73 ± 3 μC cm^{-2}, which appears to correspond to the formation of a full monolayer of oxidized thiol molecules. A further increase of the preconcentration time still produces dramatic changes in wave II, which shifts to more negative potentials and, simultaneously, becomes narrower and higher (Figure 2c). Because the number of oxidized molecules remains constant, these morphological changes are indicative of a surface reorganization process leading to an increase of the attractive interactions among the thiol molecules in the monolayer. The time required for the completion of this surface rearrangement process has been found to increase as the thiol concentration or the temperature are decreased; a typical time scale of ∼100 s corresponds to the experimental conditions in Figure 2. The final spike-like shape of wave II is consistent with a strong interaction between adsorbed molecules, whose desorption might involve a nucleation and growth mechanism.[26,27]

Some aspects of MHOL oxidation have been described before in the literature in relation with the electrochemical behavior of other organothiols. The presence of multiple waves was already reported in the seminal work of Kolthoff and co-workers,[15] although the exact nature of the oxidized products has remained unclear. Recently, White and co-workers[20] found that the oxidation of *n*-alkanethiols (with $n \geq 6$) on mercury gives rise to two well-resolved voltammetric waves, which they ascribed to two distinct surface states of the oxidized products. The occurrence of a monolayer reorganization process has also been invoked by Mandler and co-workers[6] in the case of *n*-alkanethiols and ω-mercaptocarboxylic acids.

Because of its sensitivity to the thickness and dielectric properties of the adsorbed layer, the differential capacity C_d is commonly used as a source of information about the electrode−solution interfacial structure. Figure 3 illustrates its variation with the preconcentration time for three MHOL concentrations at the deposition potential (−0.3 V). A smooth decay is always observed, leading ultimately to a limiting value of ∼4.3 μF cm^{-2}, which is typical of densely packed monolayers of functionalized alkyl chains such as alkanethiols[6,10] and fatty alcohols.[28] Similar differential capacity transients have been reported for the adsorption of nonanoic acid[29] and a series of ω-mercaptocarboxilyc acids[19] on mercury and *n*-alkanethiols on gold.[30] We have observed that down to a value of ∼12 μF cm^{-2} C_d decreases linearly with $t^{1/2}$ and its slope is proportional to the MHOL concentration, suggesting that the deposition process

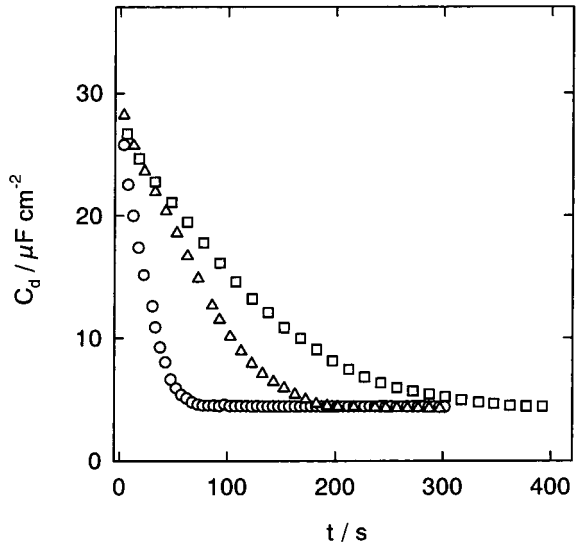

Figure 3. Differential capacity transients corresponding to (□) 7, (△) 10, and (○) 20 μM MHOL solutions in 0.5 M NaOH. Each curve is the average of four transients recorded at $f = 320$, 620, 2020, and 4020 Hz with $\Delta E_{AC} = 10$ mV.

is governed by the mass transport from the solution. This observation rules out the possibility of a nucleation and growth-type deposition mechanism, for which a sigmoidal dependence of C_d on t is to be expected.[31,32] Moreover, there is no evidence for a sudden change in the C_d transient to be associated with the development of wave II, suggesting the absence of a 2D solid-like structure as the source of this voltammetric feature. More surprisingly, C_d no longer varies during the final surface reorganization process, indicating that this process should involve only small structural changes in the monolayer, such as the loss of ions or solvent molecules from the outer part of the organic film.

Determination of Surface Concentrations. To develop a quantitative interpretation of the voltammetric features associated to the electrochemical formation of MHOL oxidized monolayers, a reliable procedure to estimate adsorbate surface concentrations is required. Surface concentration values derived from integration of the voltammetric waves, using a baseline extrapolation for the subtraction of the nonfaradaic current, can be considered only as approximate, because of the difficulty to account properly for the coupling between the faradaic and nonfaradaic components of the charge flow.[33−35] To overcome this difficulty, we have modified the classical cathodic stripping voltammetry protocol to include the possibility of an expansion/contraction of the electrode area at the end of the preconcentration time, as described in the Experimental Section. In agreement with the results of numerical simulations (see the last section), we have verified that electrode expansion does not involve a significant change in the number of oxidized thiol molecules, because the area variation takes place in a short time and in the presence of a strongly depleted concentration gradient of reduced thiol molecules in solution.

Integration of the cathodic trace, from an initial potential E_i to a final potential E_f located in the nonfaradaic region that follows the reductive desorption peaks, gives an overall charge Q_T, which consists of a faradaic Q_f and a nonfaradaic Q_{nf} component:

$$Q_T(E_i,E_f) = Q_f(N_{ox}) + Q_{nf}(N_{ox},A,E_i,E_f) \quad (1)$$

where Q_{nf} depends on the number of oxidized molecules N_{ox}, the electrode surface area A, and the potential interval $[E_i,E_f]$. Because the nonfaradaic charge is proportional to the electrode area for a given surface composition, it may be expressed as

$$Q_{nf} = q_{nf}(N_{ox},A,E_i,E_f)A \quad (2)$$

On the other hand, the faradaic component Q_f depends just on N_{ox}:

$$Q_f = nFN_{ox} \quad (3)$$

where n is the number of electrons exchanged per thiol molecule during its reductive desorption and F is Faraday's constant.

In an expansion/contraction experiment, N_{ox} remains constant, whereas A is being modified systematically. Then, the different dependence of Q_f and Q_{nf} on the electrode area can be exploited to obtain Q_f from the slope of a Q_TA^{-1} vs A^{-1} plot, at a given preconcentration time. In the case of MHOL, Q_TA^{-1} was found to vary linearly with A^{-1} (Figure 4a), so that q_{nf} in eq 2 can be considered to be independent of the electrode area. For short preconcentration times (i.e., low values of N_{ox}), the intercepts in Figure 4a were identical to the q_{nf}^0 value derived from integration of the supporting electrolyte voltammogram. These intercepts decrease slightly as the preconcentration time increases, and they are reduced by ~6% upon adsorption of a full monolayer of oxidized thiol.

Thiol surface concentrations Γ_{ox}, derived from Q_f values by assuming $n = 1$ in eq 3, have been plotted in Figure 4b as a function of preconcentration time for the 7, 10, and 20 μM MHOL solutions in 0.5 M NaOH. They display the typical response to be expected for a diffusion-limited oxidative adsorption process. Therefore, the dependence of Γ_{ox} on time is insensitive to the details of the surface oxidation mechanism, and it can be quantitatively interpreted in terms of the simplified overall reaction:

$$R_{dis} \rightleftarrows Ox_{ads} + 1e^- \quad (4)$$

where R_{dis} stands for the reduced form of MHOL in solution and Ox_{ads} stands for any of its oxidized surface states, and it has been assumed a one electron flow per oxidized thiol molecule, in agreement with the low value of q_{nf} and the results of the thermodynamic analysis of White and co-wokers.[20] In fact, the full lines in Figure 4b demonstrate that the adsorption rate can be described by considering just the finite adsorbate size, through a Langmuir adsorption isotherm, and a thiol diffusion coefficient value of $D_{MHOL} = 4.8 \times 10^{-6}$ cm^2 s^{-1}. At long enough preconcentration times, Γ_{ox} reaches a steady value equal to $\Gamma_{ox}^{max} = 6.9 \pm 0.3 \times 10^{-10}$ mol cm^{-2}, which is independent of the MHOL bulk concentration and is similar to that reported for *n*-alkanethiolate monolayers deposited on Hg.[11] This Γ_{ox}^{max} value corresponds to a projected molecular area of ~24 Å^2, in agreement with a nearly perpendicular orientation of the adsorbed thiol molecules in state II (see Figure 8).

The Desorption Waves as a Probe of Adsorbed MHOL Oxidized Molecules. *(a) Wave I.* The voltammetric features of wave I, such as the scan rate or surface concentration dependence of the peak parameters, are similar to those described previously for the reductive desorption of submonolayers of some ω-mercaptocarboxylic acids,[24] and they can be interpreted

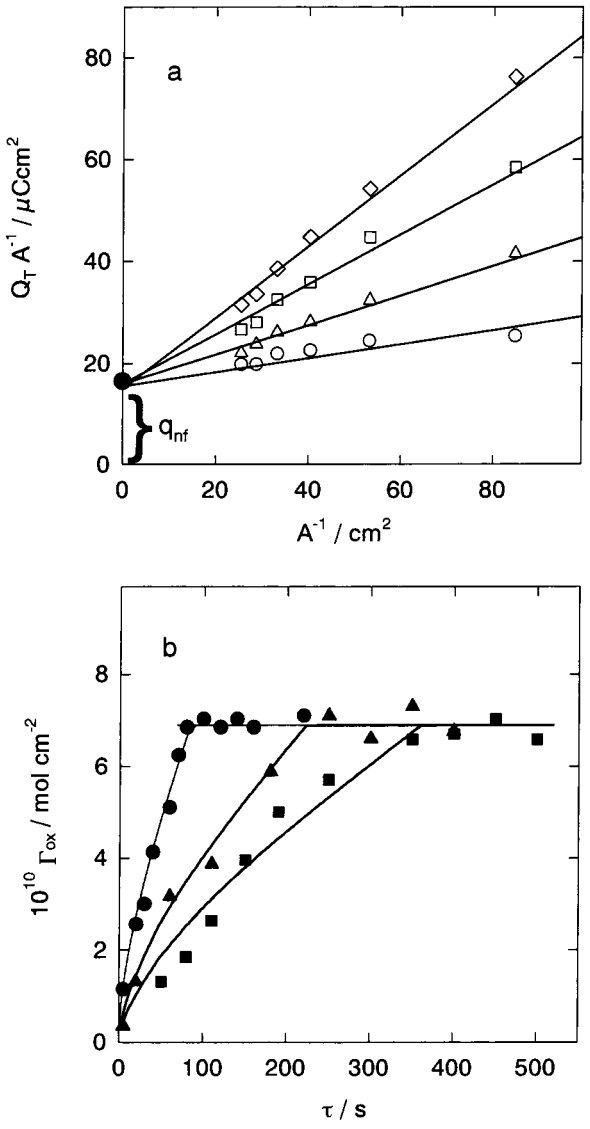

Figure 4. (a) Plot of the overall charge density, obtained by integration of the cathodic trace between −0.3 and −1.1 V (SSCE), vs the reciprocal of the electrode surface area as a function of the preconcentration time τ = (○) 5, (△) 30, (□) 60, and (◇) 80 s. The electrode surface area was varied by expanding the HMDE at the end of the preconcentration time. The slope provides an estimate of the faradaic component Q_f. The filled symbol corresponds to the charge density in the absence of thiol. (b) Surface concentrations of oxidized thiol vs the preconcentration time for (■) 7, (▲) 10, and (●) 20 μM MHOL solutions in 0.5 M NaOH. Solid lines represent theoretical fits for D_{MHOL} = 4.8 × 10^{-6} cm^2 s^{-1} and Γ_{ox}^{max} = 6.9 × 10^{-10} mol cm^{-2}.

in terms of the following surface electrodimerization mechanism:

$$R_{dis} + MS \overset{K_{a,R}}{\rightleftharpoons} MR + S_{dis}$$

$$MR \overset{E_s}{\rightleftharpoons} MO + 1e^-$$

$$MO + MO \overset{K_d}{\rightleftharpoons} MZ_I \qquad (5)$$

where the subscript dis refers to a species in solution and its absence indicates an adsorbed species. R stands for the reduced form of the MHOL molecule ($^-S(CH_2)_6OH$, in alkaline solution), MO stands for the oxidized monomer (Hg $S(CH_2)_6OH$), MZ_I stands for the oxidized dimer ($Hg_2(S(CH_2)_6OH)_2$ or Hg-$(S(CH_2)_6OH)_2$), S_{dis} stands for a solvent cluster removed upon adsorption of R_{dis}, and MS stands for a solvent cluster adsorbed

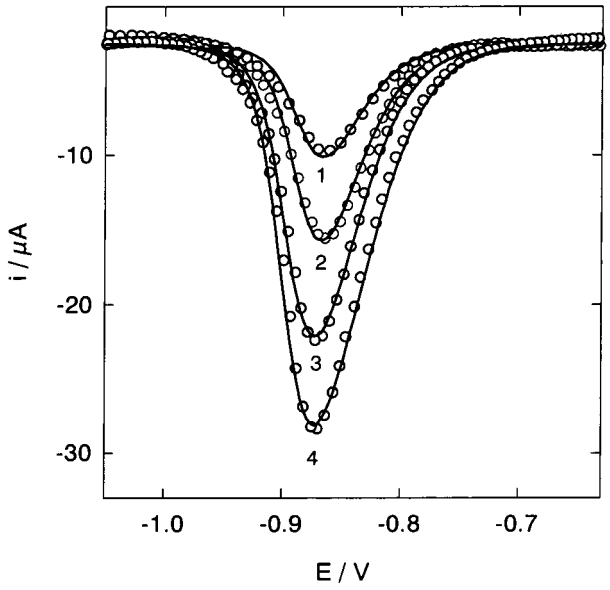

Figure 5. Comparison between experimental (○) and theoretical (solid lines) cathodic stripping voltammograms for a 20 μM MHOL solution in 0.5 M NaOH as a function of τ (s) = 1 (1), 3 (2), 7 (3), and 12 (4). υ = 10 V s^{-1}, E_i = −0.3 V. Theoretical curves were derived from reaction scheme 5 with the following parameter values: D_{MHOL} = 4.8 × 10^{-6} cm^2 s^{-1}, $E_s - RT/F \ln K_{ar}$ = −1.11 V (SSCE), $K_{aR} < 10$, K_d = 2 × 10^{10} mol^{-1} cm^2 and $\Gamma_O^{max} = 2\Gamma_{Z_I}^{max}$ = 3 × 10^{-10} mol cm^{-2}.

on reduced metal atoms. $K_{a,R}$ is the adsorption coefficient of R_{dis}, K_d is the dimerization equilibrium constant, and E_s stands for the standard potential of the charge-transfer step. It should be noted that structural evidences of thiol dimerization following its oxidative adsorption on gold have been reported previously,[36−38] whereas the presence of surface dimerization equilibria upon adsorption on mercury is substantiated by voltammetric experiments[23,24] and by the identification of the final oxidation products.[17]

Assuming that the adsorbed state can be described by a multicomponent Langmuir isotherm and that $\Gamma_O^{max} = 2\Gamma_{Z_I}^{max}$, the analysis (as described in ref 24 in detail) of the peak potential $E_{p,I}$ and half-height width w_I dependence on Γ_{ox} gives the following estimates of the relevant mechanistic parameters: $E_s - RT/F \ln K_{a,R}$ = −1.11 V(SSCE), $K_{a,R} < 10$, K_d = 2 × 10^{10} mol^{-1} cm^2, and $\Gamma_O^{max} = 2\Gamma_{Z_I}^{max}$ = 3 × 10^{-10} mol cm^{-2}. Figure 5 shows how these parameter values give a quantitative account of wave I at low enough scan rates (<100 V s^{-1}), so that individual steps in reaction scheme 5 remain in equilibrium.

Therefore, in the early stages of the electrodeposition process (i.e., when $\Gamma_{ox} \leq 3 \times 10^{-10}$ mol cm^{-2}), oxidized MHOL molecules form a mixture of monomeric and dimeric species, occupying ca. twice the surface area expected for a closed-packed array of adsorbed sulfur heads. Thus, in state I, each adsorbed monomer, or dimer, would be surrounded by reduced metal sites, which are covered by hydrocarbon chains (see Figure 8).

(b) Wave II. According to the above interpretation, wave II can be associated to the reductive desorption of additional oxidized MHOL molecules (in excess of 3 × 10^{-10} mol cm^{-2}), which are adsorbed on the reduced metal sites located between oxidized sulfur heads. This further adsorption requires a rearrangement of the previously adsorbed hydrocarbon tails. Moreover, the increase of the thiol surface concentration shifts the dimerization equilibrium toward the formation of new dimeric species, which are now restricted to occupy a smaller surface area. Because the maximum thiol surface concentration

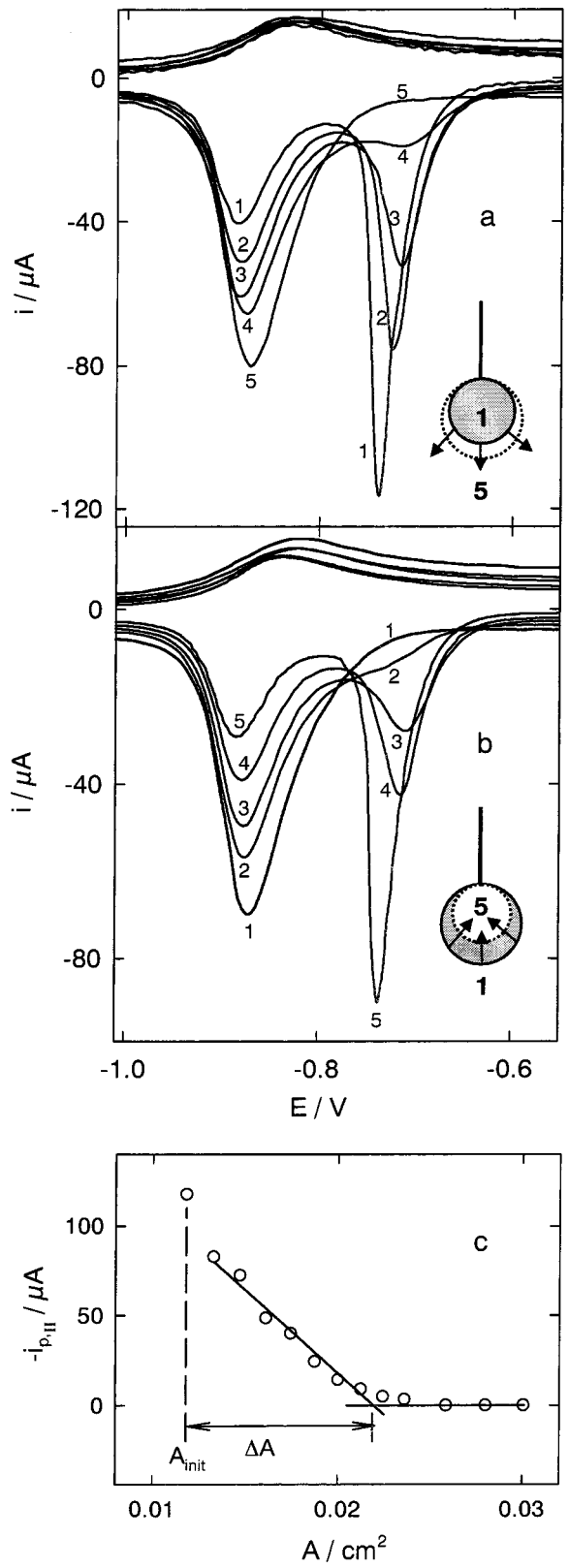

Figure 6. Influence of (a) expansion and (b) contraction of the electrode area on the cathodic stripping voltammograms of a 20 μM MHOL solution in 0.5 M NaOH. $\upsilon = 10$ V s^{-1}, $E_i = -0.3$ V. Experimental conditions in (a): $\tau = 70$ s, $A_{init} = 0.0118$ cm^2, ΔA(cm^2) = 0 (1), 2.9×10^{-3} (2), 5.6×10^{-3} (3), 8.3×10^{-3} (4), 0.0183 (5). Experimental conditions in (b): $\tau = 15$ s, $A_{init} = 0.0247$ cm^2, ΔA(cm^2) = 0 (1), -5.9×10^{-3} (2), -8.5×10^{-3} (3), -0.0114 (4), -0.0145 (5). (c) Illustration of the method used to determine the minimal expansion ΔA required to convert oxidized thiol molecules from state II to state I.

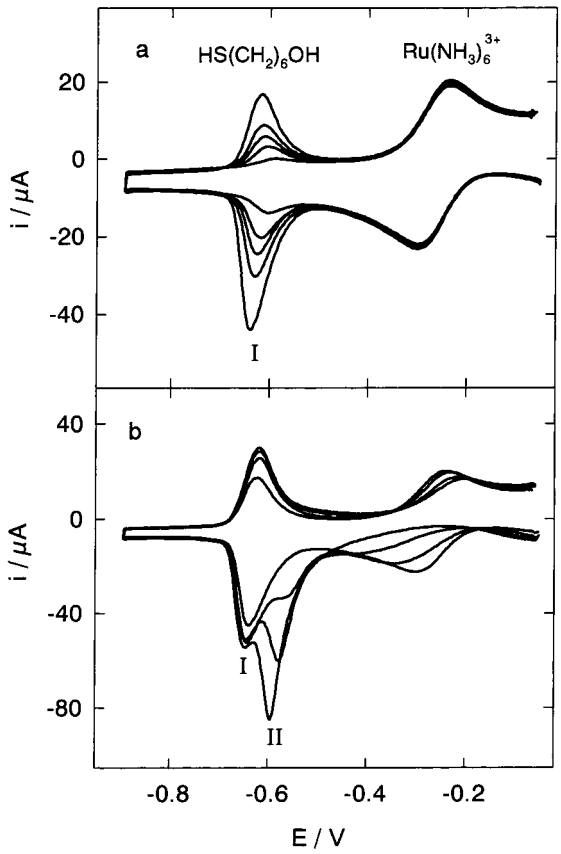

Figure 7. Cathodic stripping voltammograms of a 1 mM $Ru(NH_3)_6^{3+}$ and 10 μM MHOL solution in 0.25 M H_3PO_4 − 0.06 M $NaClO_4$ (pH = 7), as a function of τ = (a) 2, 10, 30, 50, and 70 s and (b) 80, 150, 200, and 250 s. $\upsilon = 10$ Vs^{-1}, $E_i = -0.3$ V (SSCE).

in state I (3×10^{-10} mol cm^{-2}) is ca. half of the thiol surface concentration in the compact monolayer (6.9×10^{-10} mol cm^{-2}), this last process can be represented by the following reaction:

$$MZ_I + S_{dis} \overset{K_r}{\rightleftharpoons} MZ_{II} + MS \qquad (6)$$

where Z_I stands for the previous low surface-density dimer, occupying a surface area per molecule A_{Z_I}, and Z_{II} stands for the high surface-density dimer, occupying a surface area $A_{Z_{II}}$, with $A_{Z_I} > A_{Z_{II}}$ (Figure 8). MS represents reduced metal sites that were previously hidden by the hydrocarbon chains. It should be noted that the analogous reaction involving monomers (i.e., MO + MO + $S_{dis} \leftrightarrow MZ_{II}$ + MS) is already accounted for by combining the third step of reactions 5 with 6.

To interpret the oxidative adsorption of *n*-alkanethiolates on Hg[20] and Ag(111),[22,23] White and co-workers have invoked the existence of two surface redox processes, associated with distinct energetic and packing density characteristics. Under equilibrium conditions, when reactant adsorption is negligible ($K_{a,R} \rightarrow 0$) and the dimerization equilibrium constant takes a high value ($K_d \rightarrow \infty$), the combination of reactions 5 and 6 can indeed be written as two surface redox processes:

$$2R_{dis} + 2MS \overset{E_{s,I}}{\rightleftharpoons} MZ_I + 2S_{dis} + 2e^-$$

$$2R_{dis} + MS \overset{E_{s,II}}{\rightleftharpoons} MZ_{II} + S_{dis} + 2e^- \qquad (7)$$

where the first electrode reaction results from the summation of the three elementary steps in reaction 5 and the second

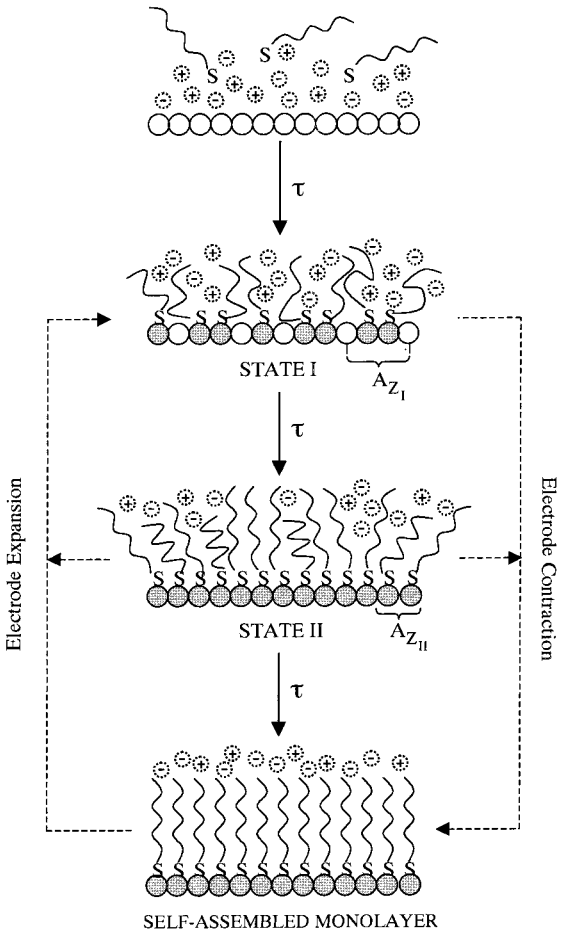

Figure 8. Schematic representation of the three states developed during the electrodeposition process of MHOL on Hg and their interconversion upon increasing the preconcentration time or varying the electrode surface area. Open and filled circles represent the reduced and oxidized metal sites, respectively.

reaction is obtained by a further addition of reaction 6. Because of their different order with respect to the free surface coverage (θ_S), the first process is favored at lower preconcentration times, where θ_S is high, and the second reaction is favored at high thiol surface concentrations, where θ_S is small. According to the relative values of their standard potentials, one ($E_{s,I} > E_{s,II}$) or two ($E_{s,I} < E_{s,II}$) voltammetric waves are to be expected. In the first case, only the species MZ_{II} would be formed at any preconcentration time. In this work, we have adopted a formalism based on the combination of reactions 5 and 6, because, as it will be shown later, it allows for a straightforward interpretation of the expansion/contraction experiments described below.

To prove the occurrence of reaction 6, and to explore its reversibility, we have performed experiments where the free surface coverage θ_S was deliberately modified by changing the electrode area, whereas the number of oxidized MHOL molecules N_{ox} was kept constant. Figure 6a shows the effect of a gradual expansion of the electrode on the voltammetric features of MHOL, under conditions where waves I and II were initially present. As can be seen, the increase of free space results in the conversion of the high surface-density dimer (wave II) into the low-surface density mixture (wave I), as expected from a shift of equilibrium (6) to the left-hand side. The corresponding experiments for the gradual contraction of the electrode are illustrated in Figure 6b. In this case, the opposite trend was observed as the electrode area was decreased, i.e., a progressive conversion of adsorbed molecules from state I to state II. These results show that reaction 6 is fast and reversible within the time scale of the motor driven expansion/contraction (from 90 to 450 ms, according to the area change).

The electrochemical stripping process bears some similarities with the mechanical expansion experiment, because in both cases free sites are generated at the electrode surface. Even when the monoloyer contains Z_{II} dimers only, the free sites generated by its voltammetric desorption will induce the formation of an intermediate state I mixed monolayer, providing thus a simple explanation for the presence of wave I at any preconcentration time.

Expansion experiments can also be used to test our previous estimate of the maximum surface concentration of thiol molecules in state I. For the monolayer-coated electrode, the number of oxidized MHOL molecules in state II can be written as

$$N^{II}_{MHOL} = A_{init} N_A \Gamma^{max}_{Z_{II}} \quad (8)$$

where N_A is the Avogadro number and A_{init} is the initial electrode area. If ΔA represents the minimal expansion of the electrode surface area which is required to convert all of the molecules in state II to state I, i.e., to cause wave II to disappear, and because the number of adsorbed thiol molecules remains constant in an expansion experiment, it follows that

$$N^{II}_{MHOL} = N^{I}_{MHOL} = (A_{init} + \Delta A) N_A \Gamma^{max}_{Z_I} \quad (9)$$

Then, by combining eqs 8 and 9 one obtains

$$\Gamma^{max}_{Z_I} = \frac{A_{init}}{A_{init} + \Delta A} \Gamma^{max}_{Z_{II}} \quad (10)$$

This expression allows us to estimate $\Gamma^{max}_{Z_I}$ from the knowledge of A_{init}, ΔA, and $\Gamma^{max}_{Z_{II}}$. We have measured ΔA (Figure 6c) for different choices of A_{init} between 8×10^{-3} cm^2 and 0.0225 cm^2 and obtained a value of $\Gamma^{max}_{Z_I} = 3.6 \pm 0.5 \times 10^{-10}$ mol cm^{-2}, in good agreement with our previous estimate from the analysis of wave I.

Additional structural information on the state of the adsorbed molecules can be derived from their blocking properties against the heterogeneous electron transfer of a soluble redox species. We have selected $Ru(NH_3)_6^{3+}$ as a redox probe, because it undergoes an electrochemical reduction within the potential region preceding the reductive desorption peaks of oxidized MHOL, allowing us to monitor simultaneously the state of the adsorbed thiol and its blocking efficiency. These measurements were carried out at pH 7, using as supporting electrolyte a mixture of the $H_2PO_4^-|HPO_4^{2-}$ buffer and $NaClO_4$ to fix the ionic strength to 0.5 M.

Figure 7 shows the evolution of the voltammetric features of a solution containing 10 μM MHOL and 1 mM $Ru(NH_3)_6^{3+}$ as a function of the preconcetration time. For low MHOL surface concentrations, when only oxidized MHOL molecules in state I exist, a reversible $Ru(NH_3)_6^{3+}/Ru(NH_3)_6^{2+}$ wave ($\Delta E_p \sim 60$ mV) is observed, whose shape does not vary upon increasing MHOL surface concentration (Figure 7a). The absence of charge transfer inhibition suggests that the adsorbed structure in state I is fully permeable to the redox couple. However, dramatic changes in the $Ru(NH_3)_6^{3+}/Ru(NH_3)_6^{2+}$ waves are observed as soon as the second reductive desorption wave of oxidized MHOL appears (Figure 7b). Now, upon increasing the surface concentration of oxidized thiol, the reduction peak of Ru-

$(NH_3)_6^{3+}$ evolves, first to a sigmoidal shape and later to an exponential dependence on potential. The sigmoidal response is characteristic of a redox process occurring on a random array of disk microelectrodes, under conditions where individual diffusion layers do not overlap.[39−41] For the present system, this might correspond to a random distribution of micropores, created by ionic permeation as the potential becomes more negative. On the other hand, the exponential shape indicates that electron tunneling across the monolayer controls the overall rate of reduction,[10,11,42,43] and it suggests that adsorbed molecules in state II adopt a close-packed arrangement, which hampers ionic permeation, at least during the actual voltammetric time scale (∼20 ms).

Theoretical Model for the Two Desorption Waves. In this section, we will describe a theoretical model that provides a quantitative interpretation of the two voltammetric waves obtained from the reductive desorption of oxidized MHOL molecules under electrochemical equilibrium conditions. Kinetic aspects related to the monolayer formation, and to the following surface reorganization process, will not be considered here and will be the subject of a future communication.

The increase of oxidized MHOL molecules leads to the formation of two adsorbed dimers Z_I and Z_{II}, that differ in their packing density, as described by the following combination of reactions 5 and 6:

$$\begin{gathered} R_{dis} + MS \overset{K_{a,R}}{\rightleftharpoons} MR + S_{dis} \\ MR \overset{E_s}{\rightleftharpoons} MO + 1e \\ MO + MO \overset{K_d}{\rightleftharpoons} MZ_I \\ MZ_I + S_{dis} \overset{K_r}{\rightleftharpoons} MZ_{II} + MS \end{gathered} \tag{11}$$

The voltammetric response associated to this reaction mechanism has been obtained under the following assumptions: (i) only the reduced form of the thiol (R_{dis}) is present in solution and can diffuse to the electrode surface, (ii) interactions between adsorbed molecules in state I (R, O, and Z_I) are negligible, whereas attractive interactions between Z_{II} dimers play a significant role in the stability of state II, and (iii) the reactant adsorption equilibrium obeys to a multicomponent Langmuir isotherm. Under these assumptions, the boundary value problem involves Fick's second law in spherical coordinates:

$$\frac{\partial c_R}{\partial t} = D_R \frac{\partial^2 c_R}{\partial r^2} + \frac{2D_R}{r}\frac{\partial c_R}{\partial r} \tag{12}$$

with the following initial and boundary conditions:

$t = 0$, $r \geq r_0$:

$$c_R(r,0) = c_R^b \tag{13}$$

$$\Gamma_R(0) = \frac{K_{a,R} c_R^b \Gamma_R^{max}}{c_S^b + K_{a,R} c_R^b} \tag{14}$$

$$\Gamma_O(0) = \Gamma_{Z_I}(0) = \Gamma_{Z_{II}}(0) = 0 \tag{15}$$

$t > 0$, $r = \infty$:

$$c_R(\infty,t) = c_R^b \tag{16}$$

$t > 0$, $r = r_0$:

$$D_R \left(\frac{\partial c_R}{\partial r}\right)_{r=r_0} = \frac{d\Gamma_R}{dt} + \frac{d\Gamma_O}{dt} + 2\frac{d\Gamma_{Z_I}}{dt} + 2\frac{d\Gamma_{Z_{II}}}{dt} \tag{17}$$

$$K_{a,R} = \frac{\Gamma_R(t) c_S^b}{\Gamma_S(t) c_R(r_0,t)} \tag{18}$$

$$\xi = \frac{\Gamma_O(t)}{\Gamma_R(t)} = \exp\left(\frac{nF}{RT}(E - E_s)\right) \tag{19}$$

$$K_d = \frac{\Gamma_{Z_I}(t)}{\Gamma_O^2(t)} \tag{20}$$

$$K_r = \frac{\Gamma_{Z_{II}}(t)\Gamma_S(t)}{\Gamma_{Z_I}(t) c_s^b}\Omega(\theta_{Z_{II}}) \tag{21}$$

where the factor $\Omega(\theta_{Z_{II}})$ accounts for the presence of short-range interactions in the surface layer, c_i^b is the bulk concentration of species i, and Γ_S is the surface concentration of free sites, which can be expressed in terms of the surface coverages ($\theta_i = \Gamma_i/\Gamma_i^{max}$) of the adsorbed species:

$$\Gamma_S = \Gamma_S^{max}(1 - \theta_R - \theta_O - \theta_{Z_I} - \theta_{Z_{II}}) \tag{22}$$

Because the surface layer consists of a complex mixture of adsorbates, an empirical approach was adopted to estimate the interaction factor. First, $\Omega(\theta_{Z_{II}})$ was approximated by the Frumkin factor:

$$\Omega(\theta_{Z_{II}}) = \exp(-g\theta_{Z_{II}}) \tag{23}$$

where g stands for the adsorbate−adsorbate interaction coefficient. However, it was found that a $\theta_{Z_{II}}$-independent g coefficient was unable to reproduce the experimental voltammetric response, because adsorbate interactions appear then to be either overestimated at low surface concentrations or underestimated at high surface concentrations. Unsatisfactory results were also obtained from the more elaborate expressions derived from the surface regular solution theory.[44] On the other hand, a rather simple dependence of $\Omega(\theta_{Z_{II}})$ on $\theta_{Z_{II}}^2$, such as

$$\Omega(\theta_{Z_{II}}) = \exp(-g\theta_{Z_{II}}^2) \tag{24}$$

was shown to provide a quantitative account of the $\theta_{Z_{II}}$-dependent shape of wave II. Presently, we can only speculate about the physical origin of the square $\theta_{Z_{II}}$ dependence in eq 24, which is probably related to our simplified chemical description of the surface reorientation process through eq 6. Thus, eq 6 gives a straightforward explanation of the expansion/contraction experiments, but it does not account explicitly for the interactions between adsorbed (and, perhaps, also dissolved) thiols that actually trigger the surface reorientation. Therefore, K_r was expressed as

$$K_r = \frac{\Gamma_{Z_{II}}(t)\Gamma_S(t)}{\Gamma_{Z_I}(t) c_S^b}\exp(-g\theta_{Z_{II}}^2) \tag{25}$$

The above boundary value problem was solved by using the dynamic version of the spline orthogonal collocation method described in a previous work.[24] In the absence of the last interconversion step ($K_r = 0$), reaction scheme 11 predicts a

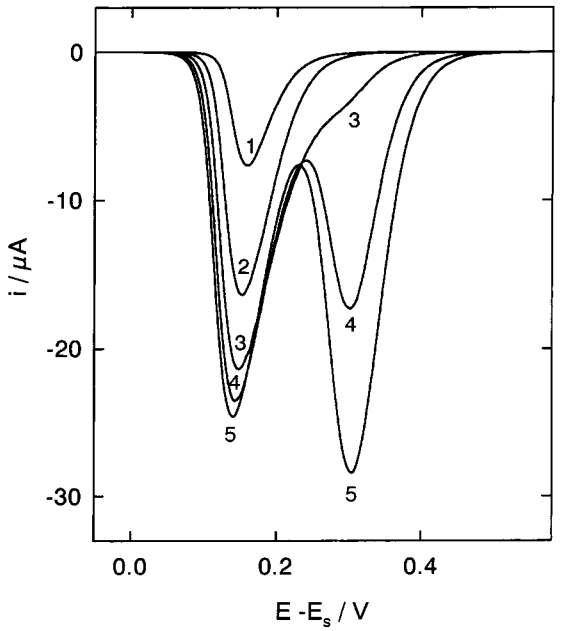

Figure 9. Simulated cathodic stripping voltammograms for reaction scheme 11 as a function of τ(s): 2 (1), 10 (2), 25 (3), 50 (4), and 75 (5). Other parameter values: $c_R^b = 10\ \mu$M, $\nu = 10$ V s^{-1}, $E_i = 0.8$ V, $E_s = 0$, $K_{aR} = 1$, $K_d = 1 \times 10^{14}$ mol^{-1} cm^2, $K_r = 1 \times 10^{-11}$ cm, $g = 0$, $D_R = 8 \times 10^{-6}$ cm^2 s^{-1}, $\Gamma_O^{max} = 2\Gamma_{Z_I}^{max} = 2 \times 10^{-10}$ mol cm^{-2}, $\Gamma_{Z_{II}}^{max} = 3 \times 10^{-10}$ mol cm^{-2}, $T = 298$ K, and $r_0 = 0.03$ cm.

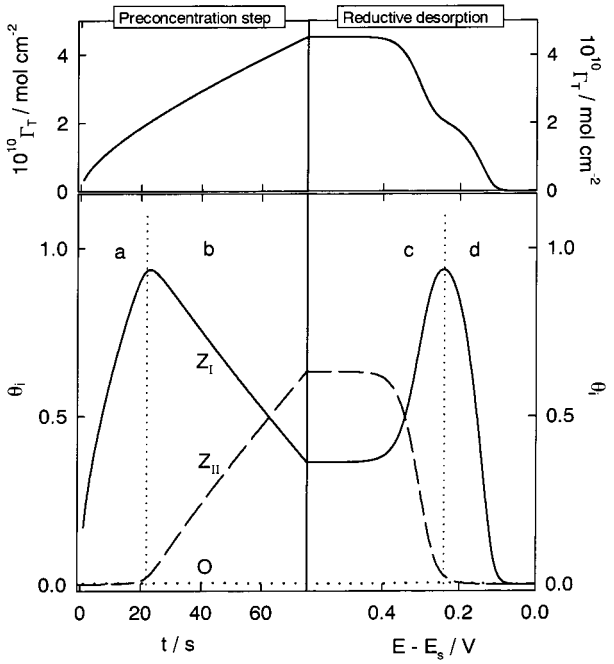

Figure 10. Evolution of the overall surface concentration Γ_T and surface coverages of oxidized species along a typical cathodic stripping experiment. (a) Formation of the low surface density layer (O, Z_I), (b) conversion of Z_I to Z_{II} by additional electrodeposition, (c) reductive desorption of Z_{II} and its conversion into a (O, Z_I) mixture, and (d) reductive desorption of the low surface density layer. $\tau = 75$ s and other parameter values as in Figure 9.

single voltammetric wave regardless of the formation of monomeric (O) or dimeric (Z_I) oxidized species.[25] From a theoretical point of view, inclusion of the low-to-high surface-density conversion step results in the appearance of a new and more anodic desorption wave, as soon as the thiol surface concentration approaches the $\Gamma_{Z_I}^{max}$ value (Figure 9). To visualize the sequence of events that take place during a typical stripping experiment according to reaction scheme 11, the surface population of each oxidized species has been plotted in Figure 10, under conditions where the two voltammetric waves are present. Four sequential processes can be distinguished: (a) the formation of a low-density adsorbed layer in the beginning of the preconcentration step (region *a* in Figure 10), (b) its conversion into a high surface-density state, which is driven by the presence of reduced thiol molecules and the lack of free sites on the surface (region *b* in Figure 10), (c) the reductive desorption of some of the high-density dimers Z_{II} and the simultaneous availability of free sites, which triggers the conversion of some Z_{II} dimers into the low-density Z_I dimers (region *c* in Figure 10), and (d) the reductive desorption of the low-density monolayer at more negative potentials (region *d* in Figure 10).

The potential gap between the two desorption waves is mainly determined by the value of the interconversion equilibrium constant K_r. A set of simulated cathodic stripping voltammograms has been plotted in Figure 11a, as a function of the K_r value. Two well-resolved voltammetric waves are observed at low K_r values, which merge into a single wave for $K_r \geq 4.5 \times 10^{-9}$ cm. Then, a further increase of K_r shifts the wave toward more cathodic potentials.

The interaction parameter g has a pronounced effect on the shape of the more anodic wave (Figure 11b). For positive g values, which may be associated to the presence of attractive $Z_{II}-Z_{II}$ interactions in the adsorbed layer, this wave becomes narrower and taller and shifts to more negative potentials upon increasing the surface concentration of Z_{II}, whereas the opposite trend is obtained for negative g values.

When the saturation coverage is reached and both waves are observed, their relative heights reflect the difference in the surface area occupied by the low- and high-density dimers A_{Z_I} and $A_{Z_{II}}$ (Figure 11c). A larger $\Gamma_{Z_{II}}^{max}/\Gamma_{Z_I}^{max} = A_{Z_I}/A_{Z_{II}}$ ratio implies that more Z_{II} molecules need to be desorbed in wave II to accommodate the low surface-density monolayer that will be reduced in wave I.

Our previous discussion has shown the adequacy of reaction scheme 11 to reproduce the main qualitative features observed in the electrochemical desorption of oxidized MHOL molecules. The next step involves the quantitative fit of the voltammetric response, and it requires a systematic comparison between the numerical solutions of the boundary value problem and the experimental voltammograms. Using the previously determined values of D_R, $\Gamma_{Z_I}^{max}$, $\Gamma_{Z_{II}}^{max}$, and $E_s - RT/F \ln K_{aR}$, and assuming that $\Gamma_R^{max} = \Gamma_O^{max} = 2\Gamma_{Z_I}^{max}$, satisfactory fits of the two voltammetric waves (Figure 12) were obtained for $K_r = 1.45 \times 10^{-11}$ cm and $g = 3.2$. Preliminary results, obtained in our laboratory for the electrochemical stripping of oxidized 4-mercaptobutanol and 11-mercaptoundecanol monolayers revealed an increase of both K_r and g with the hydrocarbon chain length, which is likely to reflect a progressive stabilization of the high-density Z_{II} dimers because of van der Waals interactions between adjacent adsorbates and favorable hydrophobic interactions.[20]

Once the surface population of each state is known, a quantitative interpretation of the differential capacity transients depicted in Figure 3 can be developed. Up to the formation of a low-density monolayer in state I, electrolyte ions, solvent, and oxidized MHOL molecules coexist in the interfacial inner layer, so that the parallel capacitors model[45] can be used to describe the dielectric properties of the interface. Then, the later incorporation of thiol molecules in state II is likely to expel

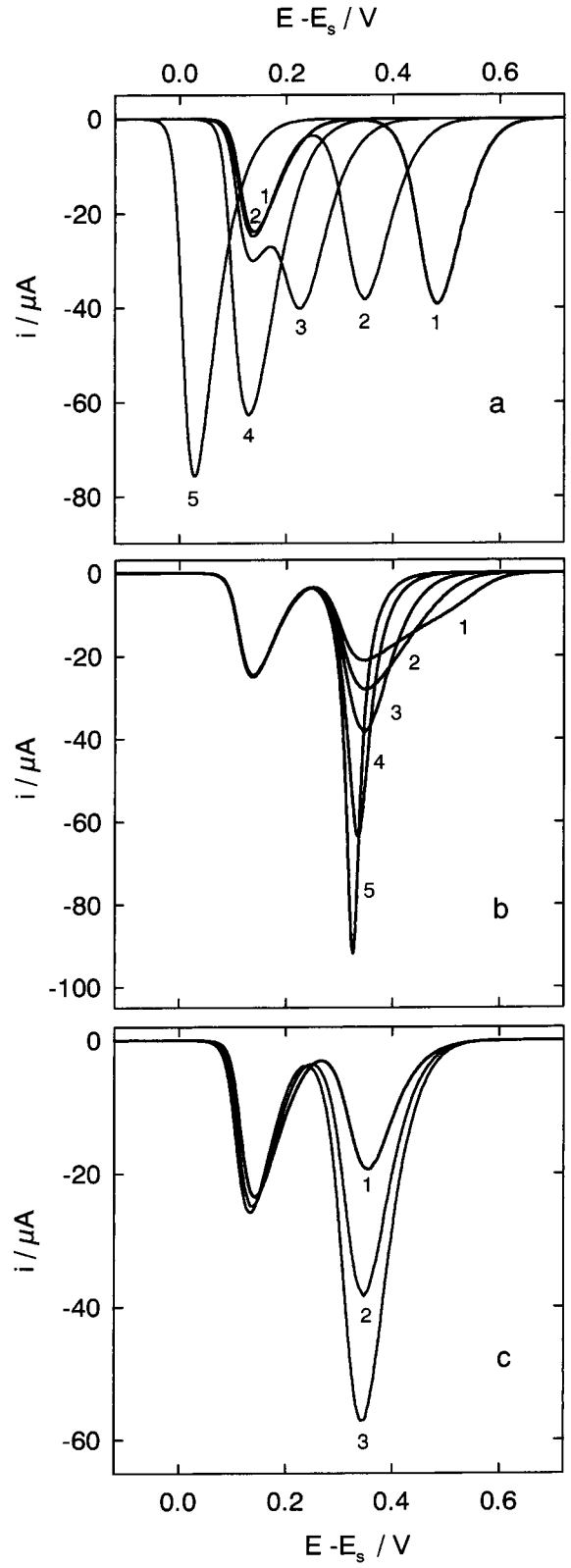

Figure 11. Simulated stripping voltammograms as a function of (a) K_r (cm): 1×10^{-14} (1), 2×10^{-12} (2), 2×10^{-10} (3), 5×10^{-9} (4), and 1×10^{-5} (5); (b) the interaction parameter g: -5 (1), -2 (2), 0 (3), 2 (4), and 3 (5); and (c) the $\Gamma_{Z_{II}}^{max}/\Gamma_{Z_I}^{max}$ ratio: 2 (1), 3 (2), and 4 (3), with $\Gamma_{Z_I}^{max} = 10^{-10}$ mol cm^{-2}. Other parameter values as in Figure 9, except for (a) $\tau = 105$ s; (b) $\tau = 105$ s and $K_r = 2 \times 10^{-12}$ cm, and (c) $\tau = 60$ s and $K_r = 2 \times 10^{-12}$ cm.

ions and solvent from the vicinity of the electrode surface and to lead to a rearrangement of the potential profile, which is best described in terms of an additional series capacitor, as illustrated

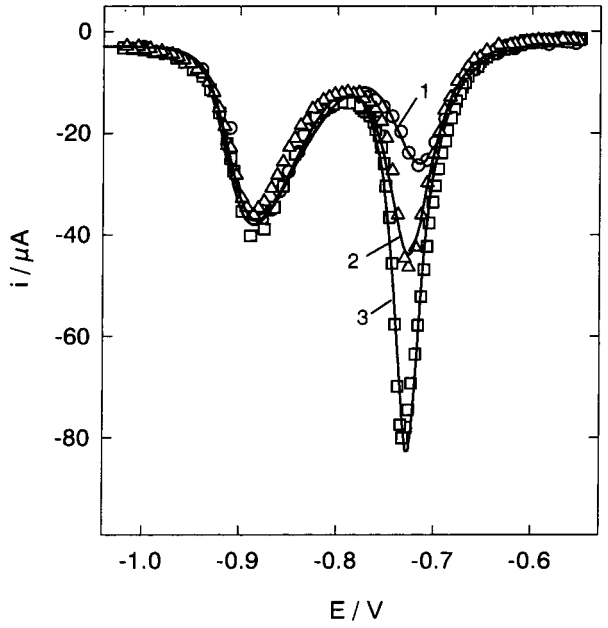

Figure 12. Comparison between experimental (open symbols) and theoretical (solid lines) stripping voltammograms for a 20 μM MHOL solution in 0.5 M NaOH, as a function of τ(s): 50 (1), 60 (2), and 80 (3). $\upsilon = 10$ V s^{-1}, $E_i = -0.3$ V. Theoretical curves correspond to the simulation of reaction scheme 11 with the following parameter values: $D_{MHOL} = 4.8 \times 10^{-6}$ cm^2 s^{-1}, $E_s - RT/F \ln K_{ar} = -1.11$ V (SSCE), $K_{aR} < 10$, $K_d = 2 \times 10^{10}$ mol^{-1} cm^2, $K_r = 1.45 \times 10^{-11}$ cm, $g = 3.2$, $\Gamma_O^{max} = 2\Gamma_{Z_I}^{max} = 3 \times 10^{-10}$ mol cm^{-2}, and $\Gamma_{Z_{II}}^{max} = 3.45 \times 10^{-10}$ mol cm^{-2}.

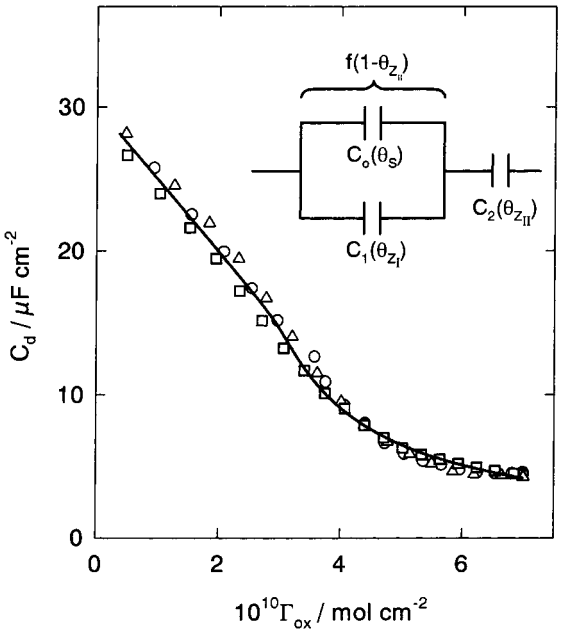

Figure 13. Differential capacity transients as a function of the thiol surface concentration Γ_{ox} for (□) 7, (△) 10, and (○) 20 μM MHOL solutions in 0.5 M NaOH. The solid line was computed from eq 27, with $C_0 = 30$, $C_1 = 15$, and $C_2 = 5.8$ μF cm^{-2} and the θ_i values derived from the optimized model parameters indicated in Figure 12. The inset shows a schematic representation of the capacitors network used to interpret the differential capacity transients.

in the inset of Figure 13. If we denote by C_0 the differential capacity of the bare electrode in the presence of the background electrolyte, and by C_1 and C_2 the differential capacities of the monolayer coated electrode in state I and state II, respectively, then the following expression for the interfacial differential

capacity at a given potential, and at any preconcentration time, is obtained:

$$\frac{1}{C_d(\tau)} = \frac{1-\theta_{Z_{II}}(\tau)}{C_0(1-\theta_O(\tau)-\theta_{Z_I}(\tau)-\theta_{Z_{II}}(\tau))+C_1(\theta_O(\tau)+\theta_{Z_I}(\tau))} + \frac{\theta_{Z_{II}}(\tau)}{C_2} \quad (26)$$

Figure 13 shows that the differential capacity transients define a unique dependence between C_d and the overall thiol surface concentration Γ_{ox}. Such dependence can be reproduced by inserting in eq 27 the previously determined θ_i values, the independent estimate of $C_0 = 30\ \mu F\ cm^{-2}$, and by considering C_1 and C_2 as adjustable parameters. Then, a satisfactory fit (full line in Figure 13) was obtained for $C_1 = 15\ \mu F\ cm^{-2}$ and $C_2 = 5.8\ \mu F\ cm^{-2}$. This last value is close to the reported capacity[28] ($5.2\ \mu F\ cm^{-2}$) for a monolayer of short-chain aliphatic alcohols perpendicularly adsorbed on a mercury surface. On the other hand, the rather high value of C_1 and the lack of significant inhibition of the $Ru(NH_3)_6^{3+}$ electron transfer suggest that thiol molecules in state I adopt a loosely ordered structure which is easily permeated by solvent and electrolyte ions (Figure 8). Finally, it should be noted that the surface rearrangement process, which follows the formation of a high density monolayer, does not have a noticeable effect on the dielectric properties of the interface. Therefore, this late stage in the self-assembling process is likely to involve a lateral rearrangement of the outer part of the hydrocarbon chains only.

Conclusions

The analysis of cathodic stripping voltammograms, capacitative transients and inhibition of $Ru(NH_3)_6^{3+}$ electron transfer has allowed the identification of three sequential states during the MHOL self-assembling process on mercury:

(a) A low surface density state, made of a mixture of noninteracting monomers and dimers of oxidized MHOL molecules, which is characterized by a single electrodimerization voltammetric wave and by its lack of influence on the rate of $Ru(NH_3)_6^{3+}$ electron transfer. The low value of the maximum surface concentration of thiol in this state (3×10^{-10} mol cm^{-2}) and the high value of the capacity corresponding to a monolayer ($15\ \mu F\ cm^{-2}$) suggest a tilted and disordered orientation of the adsorbed molecules.

(b) A high density state, made of perpendicularly oriented dimers with attractive adsorbate−adsorbate interactions, which is characterized by the presence of two consecutive desorption waves and by its ability to block $Ru(NH_3)_6^{3+}$ electron transfer. The value of the maximum surface concentration of thiol in this state (6.9×10^{-10} mol cm^{-2}) and the value of the capacity corresponding to a monolayer ($5.8\ \mu F\ cm^{-2}$) suggest the formation of a compact hydrophobic film of perpendicularly oriented adsorbates. It is also shown that the transition from the lower to the higher surface density states can be modeled as a chemical step involving the exchange of metal free sites.

(c) A SAM, made of the same number of perpendicularly oriented molecules than the high density monolayer, but with much stronger attractive interactions between adsorbed molecules, and which is characterized by the presence of a voltammetric spike. The rearrangement of a high density monolayer into a fully assembled monolayer can be monitored through the cathodic shift of the voltammetric spike. The time required for this process increases upon decreasing the thiol bulk concentration, and it was found to be ~100 s for a 20 μM thiol concentration.

Acknowledgment. This work was supported by the Spanish DGICYT under Grant PB98-1123.

References and Notes

(1) Ulman, A. *An Introduction to Ultrathin Organic Films. From Langmuir−Blodgett to Self-Assembly*; Academic Press: San Diego, CA, 1991.
(2) Dubois, L. H.; Nuzzo, R. G. *Annu. Rev. Phys. Chem.* **1992**, *43*, 437.
(3) Finklea, H. O. *In Electroanalytical Chemistry*; Bard, A. J., Rubinstein, I., Eds.; Marcel Dekker: New York, 1996; Vol. 19.
(4) Demoz, A.; Harrison, D. J. *Langmuir* **1993**, *9*, 1046.
(5) Magnussen, O. M.; Ocko, B. M.; Deutsch, M.; Regan, M. J.; Pershan, P. S.; Abernathy, D.; Grübel, G.; Legrand, J. F. *Nature* **1996**, *384*, 250.
(6) Muskal, N.; Turyan, I.; Mandler, D. *J. Electroanal. Chem.* **1996**, *409*, 131.
(7) Muskal, N.; Turyan, I.; Shurky, A.; Mandler, D. *J. Am. Chem. Soc.* **1995**, *117*, 1147.
(8) Bruckner-Lea, C.; Janata, J.; Conroy, J.; Pungor, A.; Caldwell, K. *Langmuir* **1993**, *9*, 3612.
(9) Bruckner-Lea, C.; Kimmel, R. J.; Janata, J.; Conroy, J. F. T.; Caldwell, K. *Electrochim. Acta* **1995**, *40*, 2897.
(10) Slowinski, K.; Chamberlain, R. V., II; Bilewicz, R.; Madja, M. *J. Am. Chem. Soc.* **1996**, *118*, 4709.
(11) Slowinski, K.; Chamberlain, R. V.; Miller, C. J.; Majda, M. *J. Am. Chem. Soc.* **1997**, *119*, 11910.
(12) Slowinski, K.; Slowinska, K. U.; Madja, M. *J. Phys. Chem. B* **1999**, *103*, 8544.
(13) (a) Youssefi, M.; Birke, R. L. *Anal. Chem.* **1977**, *49*, 1380. (b) MacCrehan, W. A.; Durst, R. A. *Anal. Chem.* **1978**, *50*, 2108. (c) Allison, L. A.; Shoup, R. E. *Anal. Chem.* **1983**, *55*, 8. (d) O'Shea, T. J.; Lunte, S. M. *Anal. Chem.* **1993**, *65*, 247.
(14) Turyan, I.; Mandler, D. *Anal. Chem.* **1994**, *66*, 58.
(15) (a) Kolthoff, I. M.; Barnum, C. *J. Am. Chem. Soc.* **1940**, *62*, 3061. (b) Stricks, W.; Kolthoff, I. M. *J. Am. Chem. Soc.* **1952**, *74*, 4646. (c) Kolthoff, I. M.; Stricks, W.; Tanaka, N. *J. Am. Chem. Soc.* **1955**, *77*, 5211.
(16) Miller, Y. R.; Teva, J. *J. Electroanal. Chem.* **1972**, *36*, 157.
(17) Stankovich, M. T.; Bard, A. J. *J. Electroanal. Chem.* **1977**, *75*, 487.
(18) Birke, R. L.; Mazorra, M. *Anal. Chim. Acta* **1980**, *118*, 257.
(19) Muskal, N.; Mandler, D. *Electrochim. Acta* **1999**, *45*, 537.
(20) Stevenson, K. J.; Mitchell, M.; White, H. S. *J. Phys. Chem. B* **1998**, *102*, 1235.
(21) Hatchett, D. W.; Stevenson, K. J.; Lacy, W. B.; Harris, J. M.; White, H. S. *J. Am. Chem. Soc.* **1997**, *119*, 6596.
(22) Hatchett, D. W.; Uibel, R. H.; Stevenson, K. J.; Harris, J. M.; White, H. S. *J. Am. Chem. Soc.* **1998**, *120*, 1062.
(23) Calvente, J. J.; Gil, M. L.; Andreu, R.; Roldan, E.; Dominguez, M. *Langmuir* **1999**, *15*, 1480.
(24) Calvente, J. J.; Andreu, R.; Gil, M. L. A.; Gonzalez, L.; Alcudia, A.; Dominguez, M. *J. Electroanal. Chem.* **2000**, *482*, 18.
(25) Laviron, E. In *Electroanalytical Chemistry*; Bard, A. J., Ed.; Marcel Dekker: New York, 1982; Vol. 12, p 92.
(26) Flecher, S. *J. Electroanal. Chem.* **1981**, *118*, 419.
(27) Rodriguez-Amaro, R.; Muñoz, E.; Ruiz, J. J.; Camacho, L. *J. Electroanal. Chem.* **1994**, *373*, 31.
(28) Vacheva, V.; Kaisheva, M.; Damaskin, B. *Electrochim. Acta* **1997**, *42*, 2327.
(29) Bordi, S.; Carlà, M.; Passamonti, P.; Fontanesi, C.; Pelloni, *P. Ber. Bunsen-Ges. Phys. Chem.* **1995**, *99*, 50.
(30) Subramanian, R.; Lakshminarayanan, V. *Electrochim. Acta* **2000**, *45*, 4501.
(31) Srinivasan, R.; de Levie, R. *J. Phys. Chem.* **1987**, *91*, 2904.
(32) De Levie, R. *Chem. Rev.* **1988**, *88*, 599.
(33) Schneider, T. W.; Buttry, D. A. *J. Am. Chem. Soc.* **1993**, *115*, 12391.
(34) Krysinski, P.; Chamberlain, R. V., II; Majda, M. *Langmuir* **1994**, *10*, 4286.
(35) Yang, D. F.; Wilde, C. P.; Morin, M. *Langmuir* **1996**, *12*, 6570.

(36) Fenter, P.; Eberhardt, A.; Eisenberger, P. *Science* **1994**, *266*, 1216.
(37) Yeganeh, M. S.; Dougal, S. M.; Polizzoti, R. S.; Rabinowitz, P. *Phys. Rev. Lett.* **1995**, *74*, 1811.
(38) Voets, J.; Gerritsen, J. W.; Grimbergen, R. F. P.; van Kempen, H. *Surf. Sci.* **1998**, *399*, 316.
(39) Amatore, C.; Savéant, J. M.; Tessier, D. *J. Electroanal. Chem.* **1983**, *147*, 39.
(40) Crooks, R. M.; Chailapakul, O. *Langmuir* **1993**, *9*, 884.
(41) Bilewicz, R.; Sawaguchi, T.; Chamberlain, R. V., II; Madja, M. *Langmuir* **1995**, *11*, 2256.
(42) Miller, C.; Cuendet, P.; Grätzel, M. *J. Phys. Chem.* **1991**, *95*, 877.
(43) Slowinski, K.; Slowinska, K. U.; Majda, M. *J. Phys. Chem. B* **1999**, *103*, 8544.
(44) Nikitas, P.; Pappa-Louisi, A. *Can. J. Chem.* **1986**, *64*, 328.
(45) Damaskin, B. B.; Petrii, O. A.; Batrakov, V. V. *Adsorption of Organic Compounds on Electrodes*; Plenum Press: New York, 1971.